CellPress

RUP2 facilitates UVR8 redimerization via two interfaces

Lixia Wang[1,3], Yidong Wang[1,3], Hongfei Chang[1], Hui Ren[2], Xinquan Wu[2], Jia Wen[2], Zeyuan Guan[1], Ling Ma[1], Liang Qiu[1], Junjie Yan[1], Delin Zhang[1], Xi Huang[2,*] and Ping Yin[1,*]

[1]National Key Laboratory of Crop Genetic Improvement, Hubei Hongshan Laboratory, Huazhong Agricultural University, Wuhan 430070, China

[2]State Key Laboratory of Cellular Stress Biology, School of Life Sciences, Faculty of Medicine and Life Sciences, Xiamen University, Xiamen 361102, China

[3]These authors contributed equally to this article.

*Correspondence: Xi Huang (xihuang@xmu.edu.cn), Ping Yin (yinping@mail.hzau.edu.cn)

https://doi.org/10.1016/j.xplc.2022.100428

ABSTRACT

The plant UV-B photoreceptor UV RESISTANCE LOCUS 8 (UVR8) exists as a homodimer in its inactive ground state. Upon UV-B exposure, UVR8 monomerizes and interacts with a downstream key regulator, the CONSTI-TUTIVE PHOTOMORPHOGENIC 1/SUPPRESSOR OF PHYA (COP1/SPA) E3 ubiquitin ligase complex, to initiate UV-B signaling. Two WD40 proteins, REPRESSOR OF UV-B PHOTOMORPHOGENESIS 1 (RUP1) and RUP2 directly interact with monomeric UVR8 and facilitate UVR8 ground state reversion, completing the UVR8 photocycle. Here, we reconstituted the RUP-mediated UVR8 redimerization process *in vitro* and reported the structure of the RUP2-UVR8^{W285A} complex (2.0 Å). RUP2 and UVR8^{W285A} formed a heterodimer via two distinct interfaces, designated Interface 1 and 2. The previously characterized Interface 1 is found between the RUP2 WD40 domain and the UVR8 C27 subregion. The newly identified Interface 2 is formed through interactions between the RUP2 WD40 domain and the UVR8 core domain. Disruption of Interface 2 impaired UV-B induced photomorphogenic development in *Arabidopsis thaliana*. Further biochemical analysis indicated that both interfaces are important for RUP2-UVR8 interactions and RUP2-mediated facilitation of UVR8 redimerization. Our findings suggest that the two-interface-interaction mode is adopted by both RUP2 and COP1 when they interact with UVR8, marking a step forward in understanding the molecular basis that underpins the interactions between UVR8 and its photocycle regulators.

Key words: photomorphogenesis, UV-B photoreceptor, UVR8, RUP2, COP1

Wang L., Wang Y., Chang H., Ren H., Wu X., Wen J., Guan Z., Ma L., Qiu L., Yan J., Zhang D., Huang X., and Yin P. (2023). RUP2 facilitates UVR8 redimerization via two interfaces. Plant Comm. **4**, 100428.

INTRODUCTION

As an inherent part of sunlight, UV-B (280–315 nm) plays a pivotal role in the entire life cycle of plants (Rozema et al., 1997; Heijde and Ulm, 2012; Podolec et al., 2021a). High-energy UV-B exposure induces stress responses such as DNA damage and photosynthesis inhibition, whereas low-energy UV-B irradiation plays a role in regulating plant metabolism and development (Ulm et al., 2004; Jenkins, 2009; Podolec et al., 2021a). First discovered in *Arabidopsis thaliana*, UVR8 has been characterized as the only UV-B photoreceptor identified to date (Kliebenstein et al., 2002; Rizzini et al., 2011; Yang et al., 2015). Upon UV-B absorption, ground-state UVR8 (inactive homodimer) dissociates into active monomers and rapidly interacts with the CONSTITUTIVE PHOTO-MORPHOGENIC 1/SUPPRESSOR OF PHYA (COP1/SPA) E3 ubiquitin ligase complex (Oravecz et al., 2006; Favory et al., 2009; Rizzini et al., 2011; Cloix et al., 2012; Huang et al., 2014; Yin et al., 2015;

Wang et al., 2022). This interaction in turn inhibits the E3 ligase activity of COP1/SPA against target proteins, including the central photomorphogenesis-promoting transcription factor ELONGATED HYPOCOTYL 5 (HY5), eventually triggering the expression of UV-B-responsive genes (Favory et al., 2009; Huang et al., 2013, 2014; Binkert et al., 2014; Lau et al., 2019; Han et al., 2020; Wang et al., 2022). UVR8 also directly interacts with and modulates the activities of several transcription factors, including WRKY DNA-BINDING PROTEIN 36 (WRKY36), BRI1-EMS-SUPPRESSOR 1 (BES1), BES1-INTERACTING MYC-LIKE 1 (BIM1), MYB DOMAIN PROTEIN 73/77 (MYB73 and MYB77), and MYB13, as well as the DNA methyltransferase DOMAINS REARRANGED
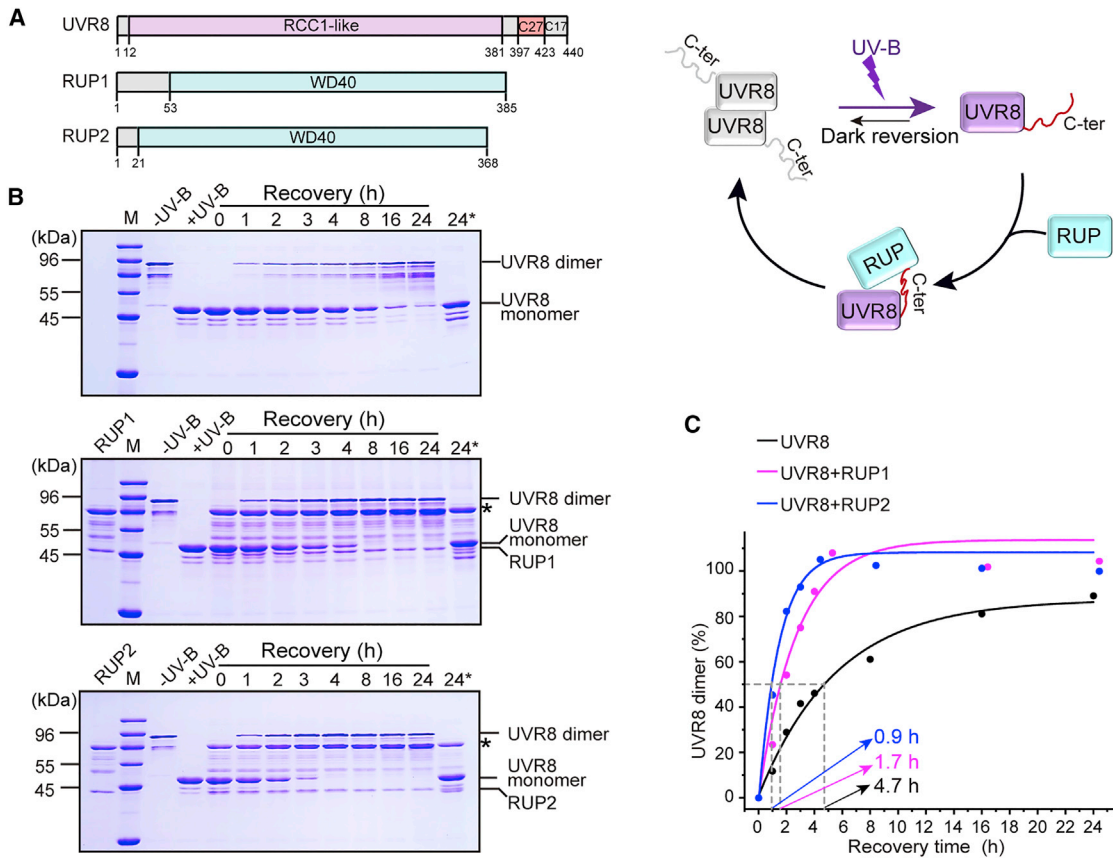
Figure 1. RUPs facilitate the redimerization of UVR8 *in vitro*.

(A) Color-coded domain structure of UVR8 and RUP1/2. UVR8 contains the N-terminal RCC1-like core domain in purple, the C27 subregion in red, and the C17 subregion in gray. RUP1/2 is composed of a short N-terminal extension in gray and a WD40 domain at the C terminus in cyan. Simplified cartoon model of the core UVR8 photocycle (right panel). Inactive UVR8, active UVR8, and RUP (RUP1/2) are colored in gray, purple, and cyan, respectively. RCC1, Regulator of Chromosome Condensation 1; C-ter, C terminus.

(B) *In vitro* reconstruction of RUP1- and RUP2-mediated facilitation of UVR8 redimerization. UV-B-activated monomeric UVR8 was subjected to dark reversion without (upper panel) or with RUP1 (middle panel) and RUP2 (lower panel) at the indicated time points. 24* indicates that redimeric UVR8 dissociates into monomers again upon UV-B irradiation. M, molecular weight ladder (kDa). Asterisk (*) indicates a contaminant protein band.

(C) Quantification of the kinetics of wild-type UVR8 homodimer regeneration without (black) or with RUP1 (magenta)/RUP2 (blue) shown in **(B)**. The solid lines indicate fitted curves. The dots indicate the percentage of redimerized UVR8 relative to total UVR8 protein without UV-B treatment at the indicated time points. The gray dashed lines indicate the time required for 50% of the UVR8 dimer to regenerate.

METHYLTRANSFERASE 2 (DRM2), thereby regulating gene transcription (Liang et al., 2018, 2019; Yang et al., 2018, 2020; Qian et al., 2020; Jiang et al., 2021).

UVR8 comprises two distinct domains: an N-terminal UV-B sensing core domain (residues 12–381) and a flexible C-terminal domain encompassing the C27 (residues 397–423) and C17 (residues 424–440) subregions (Christie et al., 2012; Cloix et al., 2012; Wu et al., 2012; Yin et al., 2015; Lin et al., 2020). The C27 subregion contains a Val-Pro (VP) motif responsible for binding to the COP1/SPA complex (Holm et al., 2001; Yin et al., 2015; Lau et al., 2019; Wu et al., 2019; Wang et al., 2022) (Figure 1A). In the ground state, UVR8 forms a bottom-to-bottom symmetric dimer via a network of salt bridges mediated by two surface patches of complementary charged residues in the core domains (Christie et al., 2012; Wu et al., 2012). Several intrinsic tryptophan residues (especially W285 and W233) located at the dimer interface serve as chromophores for UV-B perception (Christie et al., 2012; Wu

et al., 2012). It is proposed that UV-B irradiation results in excitation of the W285 and W233 indole rings, thus destabilizing the cation-π interactions and/or neutralizing the key salt bridge interactions via a proton-coupled electron transfer reaction (Christie et al., 2012; Wu et al., 2012, 2014; Li et al., 2014, 2020, 2022; Voityuk et al., 2014; Mathes et al., 2015). The destabilization and/or neutralization consequently lead(s) to the dissociation of the UVR8 homodimer into monomers (Christie et al., 2012; Wu et al., 2012, 2014; Li et al., 2014, 2020, 2022; Voityuk et al., 2014; Mathes et al., 2015; Podolec et al., 2021a).

To avoid exaggerated UV-B responses, additional regulators play roles in UVR8-mediated signaling (Podolec et al., 2021a). Two highly related WD40-repeat proteins, RUP1 and RUP2, mediate the negative feedback regulation of the UV-B response pathway (Gruber et al., 2010; Heijde and Ulm, 2013). Upon UV-B irradiation, RUPs are transcriptionally activated in a UVR8-, COP1-, and HY5-dependent manner

(Gruber et al., 2010). Overexpression of RUP2 reduces UV-B-induced photomorphogenesis and impairs UV-B acclimation (Gruber et al., 2010; Heijde and Ulm, 2013). Further investigations revealed that RUPs directly interact with UVR8 in plants and yeast, facilitate UVR8 ground state reversion in planta (redimerization of monomeric UVR8; Figure 1A), and disrupt the UVR8-COP1/SPA complex to repress UV-B signal transduction (Heijde and Ulm, 2013). However, the molecular mechanisms that underpin these processes remain largely elusive.

In this study, we reconstructed the RUP-mediated UVR8 ground state reversion *in vitro* and determined the crystal structure of RUP2 in complex with UVR8^{W285A} at a 2.0-Å resolution. Two distinct interfaces can be observed in the RUP2-UVR8^{W285A} heterodimer, in which both the UVR8 core domain and C27 subregion are involved in the interaction with RUP2. Using in planta physiological analysis and *in vitro* biochemical analyses, we found that both interaction interfaces are crucial for RUP2's function in promoting UVR8 redimerization. Our study reveals the molecular basis of RUP2-UVR8 interaction and marks a step forward in understanding how RUP2 facilitates UVR8 ground state reversion.

RESULTS

In vitro reconstruction of RUP-mediated UVR8 ground state reversion

Prior studies indicated that the *in vivo* UVR8 redimerization process takes about 2 h (Heijde and Ulm, 2013; Heilmann and Jenkins, 2013; Yin et al., 2015). During *in vitro* assays, ground state homodimeric UVR8 monomerizes upon UV-B exposure and slowly converts back to the dimeric state (~30 h) in the dark (Wu et al., 2012; Heilmann and Jenkins, 2013; Wang et al., 2022). In this study, we first determined the auto recovery rate of the UVR8 dimer in the dark after UV-B treatment. As expected, UVR8 existed as a stable dimer in the absence of UV-B and monomerized after UV-B irradiation (Figure 1B). At 24 h post UV-B treatment, approximately 90% of UVR8 monomers reverted to the dimeric form (Figure 1C). The resultant UVR8 dimer completely monomerized upon a second round of UV-B exposure, indicating that it retained UV-B sensing capability after redimerization (Figure 1B).

We then investigated whether recombinant RUP1 and RUP2 proteins had any promotive effect on UVR8 redimerization *in vitro*. Great efforts were made to express RUPs in prokaryotic and eukaryotic expression systems, but an acceptable amount of RUPs could only be obtained, along with contaminants, by expression and purification in mammalian cells (Figure 1B). When co-incubated with RUP1 or RUP2, most monomeric UVR8 reverted to the homodimeric state within 4 h, which is much faster than the UVR8 auto recovery rate (Figure 1B and 1C). These results suggest that the recombinant RUPs facilitated the reversion of UV-B-activated UVR8 to its ground state.

RUP1 and RUP2 were previously shown to interact with both monomeric and homodimeric UVR8 in plants and yeast, although they exhibited a higher affinity for the active UVR8 monomers (Gruber et al., 2010; Cloix et al., 2012; Yin et al., 2015). Thus,

we further investigated whether RUP1/2 directly interacts with UVR8 via *in vitro* pull-down assays. RUP1/2-Flag was incubated with UV-B-treated or untreated UVR8-Strep II and then pulled down using anti-Flag G1 affinity resin. UV-B-activated monomeric UVR8 was readily pulled down by RUP1/2-Flag, whereas almost no dimeric UVR8 was observed after the pull-down assays (Supplemental Figure 1A). These results suggest that RUP1 and RUP2 tend to interact with UVR8 in a UV-B-dependent manner *in vitro*.
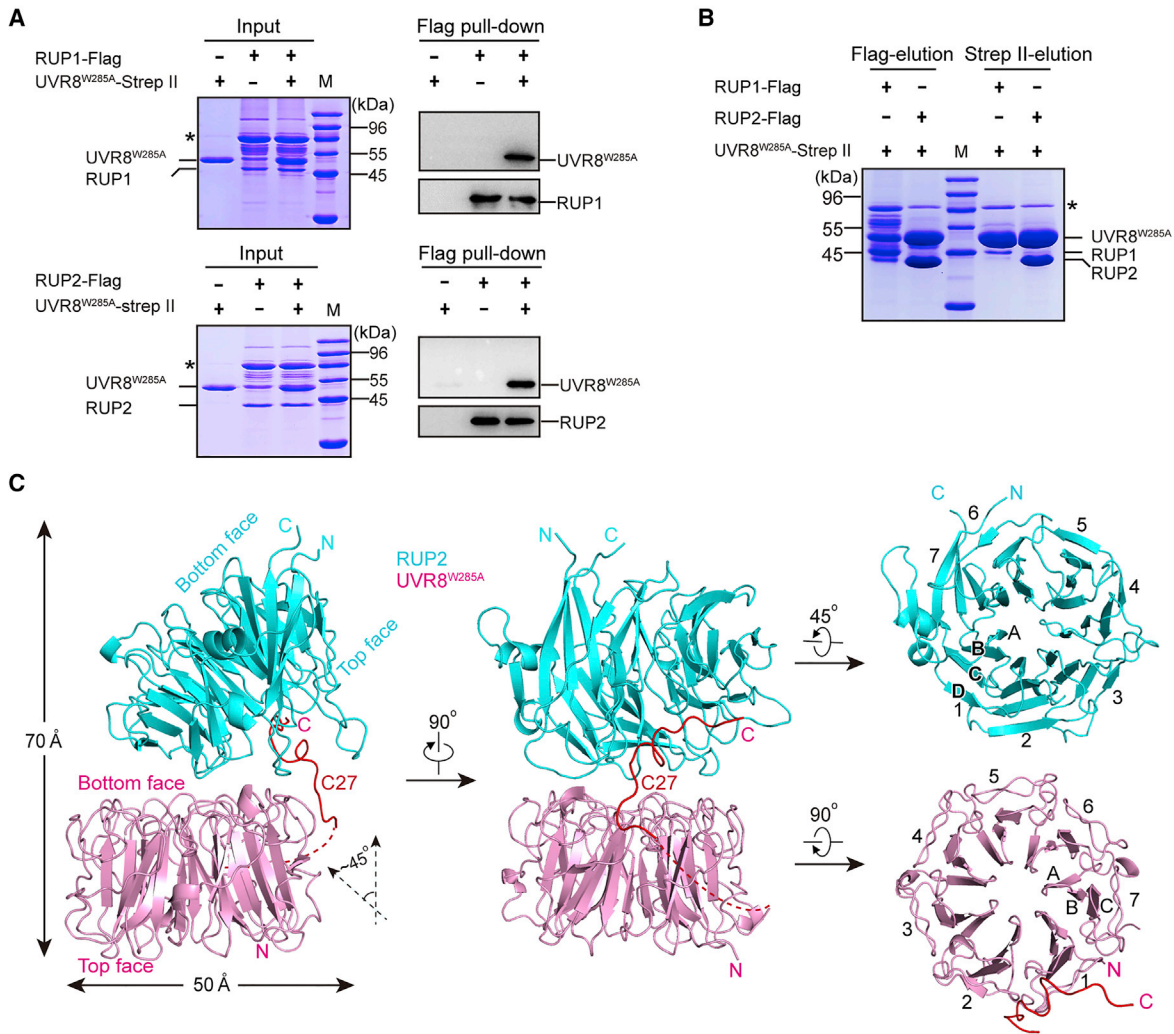
Overall structure of the RUP2-UVR8^{W285A} complex

The *in vitro* reconstruction of a stable RUP-UVR8 complex is a key step for understanding the interaction between the two proteins. We first co-expressed RUP1 (or RUP2) and UVR8 in Expi293F cells and purified the proteins under UV-B treatment. However, owing to the dynamic nature of RUP2-UVR8 interaction and UVR8 monomerization/redimerization cycles, it is difficult to obtain a relatively stable RUP2 in complex with UV-B-activated UVR8 for crystallization (Supplemental Figure 1B). A previous structural study used a constitutively activated mutant of the plant blue-light receptor cryptochrome 2 (CRY2, CRY2^{W374A}) that mimics the photoactivated conformation and elucidated how CRY2 undergoes dynamic conformational change during blue-light-induced activation (Ma et al., 2020a; Shao et al., 2020). Similarly, we chose UVR8^{W285A}, a well-known physiologically constitutively active mutant of UVR8, which results in a constitutive photomorphogenesis phenotype in the dark when overexpressed in planta, for further structural analysis (Heijde et al., 2013; Huang et al., 2014; Podolec et al., 2021b).

Consistent with previous reports (Heijde et al., 2013; Huang et al., 2014; Yin et al., 2015; Podolec et al., 2021b), *in vitro* pull-down assays showed that UVR8^{W285A} directly interacts with RUP1/2 in a UV-B-independent manner (Figure 2A). When co-expressed in Expi293F cells, UVR8^{W285A} was observed to form a complex with RUP1 or RUP2 (Figure 2B). RUP2-UVR8^{W285A} exhibited relatively higher yield compared with RUP1-UVR8^{W285A} when subjected to further purification. Furthermore, homogeneous RUP2-UVR8^{W285A} complex can be obtained after gel filtration chromatography (Supplemental Figure 2) and was thus chosen for further crystallization experiments. After numerous attempts, we finally obtained the RUP2-UVR8^{W285A} (RUP2 residues 21–366, UVR8^{W285A} residues 12–421) crystal and determined its structure at 2.0-Å resolution (Supplemental Table 1, PDB:8GQE). Overall, the RUP2-UVR8^{W285A} heterodimer has a height of approximately 70 Å and a width of 50 Å. The UVR8 β-propeller core domain (residues 12–381) and part of the C27 subregion (residues 397–413) were clearly observed, whereas the linker (residues 382–396) in between showed poor electron density, possibly due to flexibility. An ~45° angle is observed between the two central axes of the UVR8 core domain and the RUP2 WD40 domain owing to the tilt of the latter (Figure 2C).

RUP2 displays a canonical WD40 fold and interacts with UVR8^{W285A} through two interfaces

The RUP2 WD40 domain displays a canonical seven-bladed β-propeller architecture, with each blade comprising four β-strands (termed A to D) from the inner to the outer ring of the propeller (Figures 2C and 3A). The RUP2 propeller fold ends with the N-terminal β-strand (residues 25–33), which is the last

**Figure 2. Overall structure of the RUP2-UVR8^{W285A} complex.**

(A) RUP1/2 interacts with UVR8^{W285A} in a UV-B-independent manner. Purified RUP1-Flag (or RUP2-Flag) was incubated with UVR8^{W285A}-Strep II and then pulled down by anti-Flag G1 affinity resin. The input samples in the pull-down assay were analyzed by SDS-PAGE. The elution samples were detected by immunoblotting with antibodies against Flag and Strep II. M, molecular weight ladder (kDa). Asterisk (*) indicates a contaminant protein band.

(B) RUP1/2 forms a stable complex with UVR8^{W285A}. RUP1 (or RUP2) and UVR8^{W285A} were co-expressed in Expi293F cells. The proteins were purified using anti-Flag G1 affinity resin and Strep-Tactin affinity resin, respectively. The elution samples were analyzed by SDS-PAGE. M, molecular weight ladder (kDa). Asterisk (*) indicates a contaminant protein band.

(C) Crystal structure of the RUP2-UVR8^{W285A} complex. The core domain and part of the C27 subregion (residues 397–413 can be traced) of UVR8^{W285A} are indicated by pink and red, respectively. RUP2 is colored in cyan. The dotted lines indicate unresolved regions.

β-strand of the seventh blade (7D). An extended loop (residues 68–94) linking β-strands 1C and 1D (hereafter named the 1CD loop) located on the side of RUP2 contains an additional α1 (residues 69–75) and β5 (residues 84–87) (Figure 3A, 3B, and Supplemental Figure 3). β5 forms a parallel strand with β-strand 7D (Figure 3C). Two long loops extending out of the top of RUP2, one (residues 33–43) located between β-sheet 7D and 1A and the other (residues 319–335) linking β-sheet 6D and 7A (Figure 3A), encircle parts of the UVR8^{W285A} C27 subregion (Figure 3D–3F and Supplemental Figure 3).

The UVR8^{W285A} and RUP2 interactions are mediated through two interfaces, termed Interface 1 and 2, with a total buried surface area of ∼1620 Å^2 (Figure 2C). The UVR8^{W285A} C27 subregion

binds to the top of RUP2 and forms Interface 1, which has been characterized previously via yeast two-hybrid analysis and in planta mutational analysis (Cloix et al., 2012; Yin et al., 2015). Specifically, in the solved structure, the conserved VP motif from the C27 subregion anchors to a shallow RUP2 binding pocket comprising K101, L102, W148, C198, T257, and F284 (Figure 4A). Residues 400 to 413 in the UVR8 C27 subregion and their interacting counterparts of RUP2 form a network of hydrogen bonds and hydrophobic interactions (Supplemental Figure 4). Part of the C27 subregion extends out from the bottom of the UVR8 core domain and covers part of the acidic surface patch responsible for UVR8 dimer formation (Supplemental Figure 5). We performed mutational analysis and subsequent *in vitro* biochemical assays to corroborate the
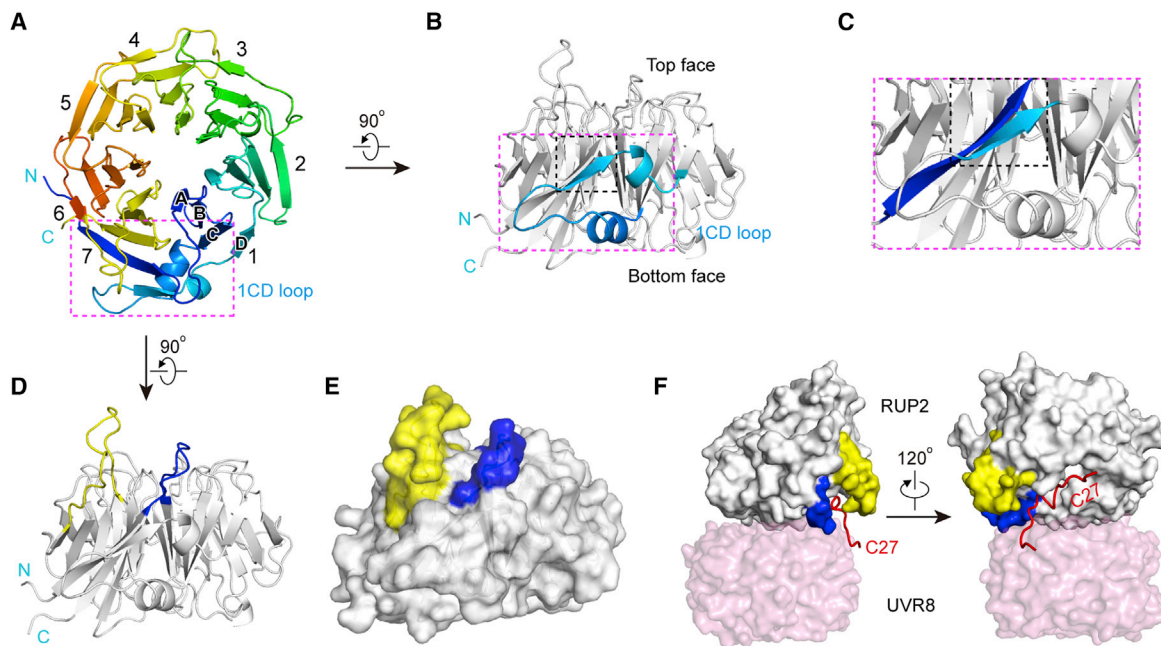
Figure 3. Structure of the RUP2 WD40 domain (RUP2^WD40).

(A) Top view of seven-bladed WD40 β-propeller of RUP2 displayed as a cartoon. The propellers are differently colored. The 1CD loop is highlighted in the magenta rectangle.

(B) Side view of RUP2^WD40. The 1CD loop is highlighted in cyan.

(C) A close-up view of β-sheet5 (cyan), which is parallel to strand 7D (blue).

(D) and **(E)** Two long loops extend out of the RUP2^WD40 top and are highlighted in blue and yellow, respectively. The structure is displayed as a cartoon **(D)** or surface **(E)**.

(F) The two long loops encircle the C27 subregion of UVR8^W285A. The C27 subregion is depicted in red.

importance of this C27 subregion. The two UVR8^W285A mutants UVR8^W285A,N396 (C-terminally truncated mutant, residues 1–396) and UVR8^W285A,VP/AA (double alanine substitutions of residues V410 and P411) lost the capacity to bind RUP2 (Figure 4B). Furthermore, like wild-type UVR8, the UVR8^N396 mutant retained the capability to monomerize upon UV-B irradiation and reverted back to the ground state autonomously in the dark, but its auto recovery rate was not affected by co-incubation with RUP2 (Figure 4C and 4D). In addition, the alanine substitutions of UVR8 residues V410 and P411 strongly impaired UVR8 redimerization in planta (Yin et al., 2015). Together, these results indicate that the UVR8 C27 subregion is crucial for RUP2-UVR8 interactions and is required for the promotion of UVR8 redimerization by RUP2 *in vitro*.

Interface 2 was found between the RUP2 WD40 domain (β-propeller blades 1 and 2) and the UVR8 core domain (β-propeller blades 1–3, 6, and 7), which contain two surface patches with complementary charges (Figure 5A, 5B, and Supplemental Figure 6A). Specifically, the RUP2 positively charged surface patch contains R62, K63, K101, and R146, and its UVR8 counterpart comprises D77, D96, D44, and E43. The acidic surface patch of RUP2 comprises D122, E138, D140, and E141, and its UVR8 counterpart contains R41, R338, R286, R354, and K304. The charged amino acids form 13 pairs of intermolecular hydrogen bonds in total (Figure 5A). The salt bridges mediated by ionic interactions between the RUP2 WD40 β-propeller and the UVR8 core domain are similar to those observed in the previously reported UVR8 homodimer, except that in the UVR8 dimer, the

charged surface patches exhibit more ionic interactions (Christie et al., 2012; Wu et al., 2012) (Figure 5C).

RUP2-UVR8 Interface 2 plays crucial roles in UVR8 redimerization

The roles of the observed ionic interactions were investigated through alanine substitutions and subsequent Flag/Strep affinity purification assays (Supplemental Figure 6B–6D). The RUP2^R62A, RUP2^D122A, RUP2^E138A, and RUP2^D140A mutants displayed dramatically reduced binding affinity to UVR8^W285A, whereas RUP2^K101A partially retained binding to UVR8^W285A (Supplemental Figure 6B). By contrast, RUP2 S40, K63A, Y95, E141, and R146A mutations had little impact on the binding of RUP2 to UVR8^W285A (Supplemental Figure 6B). Compared with these single alanine substitution mutants, the RUP2 mutant with combined D122A/E138A/D140A mutations (hereafter named RUP2^DED) exhibited a further reduction in UVR8^W285A binding affinity (Supplemental Figure 6C). Among the alanine substitutions in UVR8^W285A, only the D44A mutation of UVR8^W285A had an obvious adverse effect on the yield of RUP2 during co-expression, suggesting that this mutation potentially affected the formation of the UVR8^W285,D44A-RUP2 complex. Other UVR8 mutants retained the ability to form complexes with RUP2 (Supplemental Figure 6D).

To corroborate the importance of these key residues in planta, we generated transgenic *Arabidopsis thaliana* lines overexpressing Flag-tagged RUP2 or RUP2 mutants (RUP2^D122A or RUP2^DED)
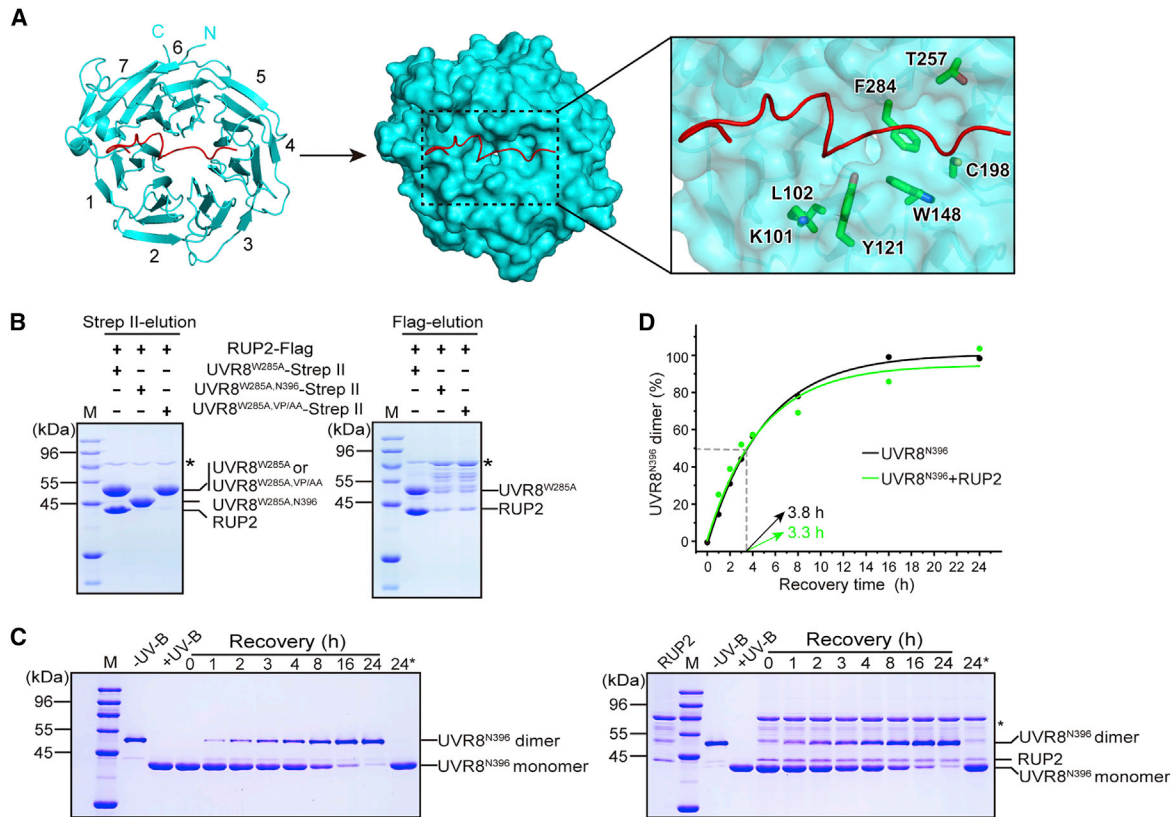
Figure 4. The C27 subregion is essential for the interaction between UVR8^{W285A} and RUP2.

(A) Top view of the C27 subregion bound to RUP2^{WD40}. RUP2^{WD40} is shown in cartoons (left panel) and as a surface (middle panel) in cyan. Close-up view of the C27 binding pocket (right panel), in which key residues are indicated by sticks in green. The C27 subregion is colored in red.

(B) Mutations in the C27 subregion disrupt the interaction between UVR8^{W285A} and RUP2. RUP2-Flag was co-expressed with UVR8^{W285A}-Strep II, UVR8^{W285A,N396} (residues 1–396), or UVR8$^{W285A,VP/AA}$ (alanine substitution of the residues V410-P411) in Expi293F cells. The proteins were purified using anti-Flag G1 affinity resin and Strep-Tactin affinity resin, respectively. The elution samples were analyzed by SDS-PAGE. M, molecular weight ladder (kDa). Asterisk (*) indicates a contaminant protein band.

(C) RUP2 has no effect on the redimerization of UVR8^{N396}. UV-B-activated monomeric UVR8^{N396} was subjected to dark reversion without (left panel) or with RUP2 (right panel) at the indicated time points. M, molecular weight ladder (kDa). Asterisk (*) indicates a contaminant protein band.

(D) Quantification of the kinetics of UVR8^{N396} homodimer regeneration without (black) or with RUP2 (green) shown in (C). The solid lines indicate fitted curves. The dots indicate the percentage of redimerized UVR8^{N396} relative to total UVR8^{N396} protein without UV-B treatment at the indicated time points. The gray dashed lines indicate the time required for 50% of the UVR8^{N396} dimer to regenerate.

in wild-type (Col) and *rup1-1 rup2-1* double mutant backgrounds (Figure 6A, 6C, and Supplemental Figure 7A), and we examined the effect of these mutations on UV-B induced photomorphogenesis. Consistent with previous reports, wild-type seedlings (Col) showed normal UV-B-dependent photomorphogenesis, and *rup1-1 rup2-1* displayed shorter hypocotyls than Col under both −UV-B and +UV-B conditions (Gruber et al., 2010; Ren et al., 2019; Podolec et al., 2021b) (Figure 6). In the wild-type background, RUP2 overexpression significantly inhibited UV-B-induced photomorphogenesis; by contrast, RUP2^{D122A} overexpression had a partially inhibitory effect, and RUP2^{DED} overexpression had no obvious inhibitory effect (Figure 6A and 6B). This was further supported by the observation that RUP2 but not RUP2^{DED} overexpression in the *rup1-1 rup2-1* background was able to rescue the short hypocotyl phenotype (line 2-2) or even displayed a UV-B-hyporesponsive phenotype (line 3-3) (Figure 6C and 6D). These results indicate that RUP2^{D122A} and RUP2^{DED} are functionally deficient RUP2 mutants with regard to plant UV-B-induced photomorphogenesis.

We further investigated the capability of RUP2^{DED} to facilitate UVR8 redimerization in planta. UVR8 monomerization rate in the *rup1-1 rup2-1* seedlings was comparable to that observed in wild-type seedlings, but UVR8 redimerization was significantly slower in the double mutant (Supplemental Figure 7B and 7C). Constitutive expression of RUP2^{DED} in the *rup1-1 rup2-1* mutant had no effect on UVR8 monomerization and redimerization compared with the *rup1-1 rup2-1* mutant, suggesting that the RUP2^{DED} mutant lost the capability to facilitate UVR8 dimerization (Supplemental Figure 7). The importance of these key residues is further supported by our previous report that RUP2^{R62A}, RUP2^{D122A}, RUP2^{E138A}, and RUP2^{D140A} failed to facilitate UVR8 ground state reversion *in vitro* (Wang et al., 2022) and by the observation that RUP2 failed to promote UVR8^{D44A} redimerization (Supplemental Figure 6E and 6F). Taken together, these results indicate that residues D122, E138, and D140 of RUP2 in Interface 2 play pivotal roles in regulating UVR8 redimerization in planta and *in vitro*.
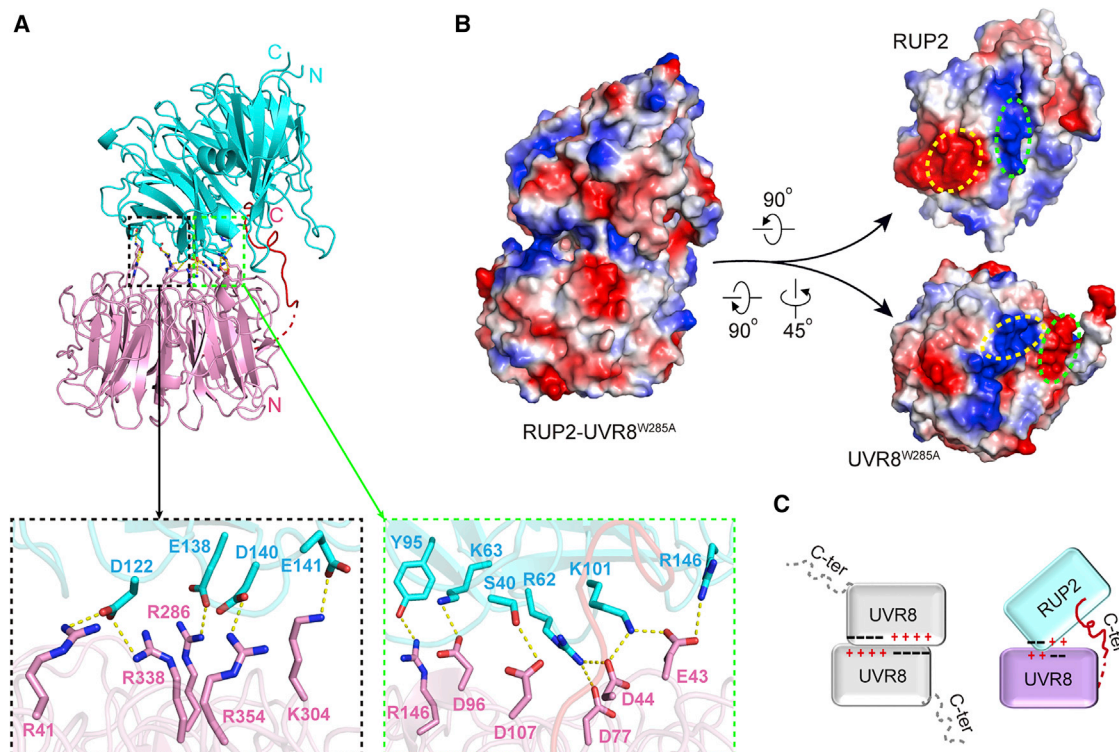
Figure 5. Interface 2 between RUP2^{WD40} and the core domain of UVR8.

(A) Close-up views of RUP2-UVR8^{W285A} Interface 2 indicated by black and green dashed boxes. Residues from RUP2 and UVR8^{W285A} are colored in cyan and pink, respectively. Hydrogen bonds are indicated by yellow dashed lines.

(B) The interaction between RUP2^{WD40} and the core domain of UVR8 is mediated by two complementary charged surfaces. The positively charged patch of RUP2 interacts with the negatively charged patch at the bottom of UVR8^{W285A} (in green) and vice versa (in yellow).

(C) Cartoon of interaction interfaces in UVR8 homodimer and RUP2-UVR8^{W285A} formation. C-ter indicates C terminus. "+" and "−" indicate positive and negative charge, respectively.

Comparison of RUP2-UVR8^{W285A} with other known UVR8-related structures

We recently reported the cryo-electron microscopy (cryo-EM) structure of the COP1 WD40 domain in complex with UV-B-activated UVR8 (COP1^{WD40}-UVR8, PDB:7VGG) (Wang et al., 2022). Intriguingly, RUP2-UVR8^{W285A} and COP1^{WD40}-UVR8 adopt a similar architecture, and COP1^{WD40} also interacts with both the UVR8 core domain and the C-terminal region (Figure 7A) (Wang et al., 2022). Superposition of the two complexes revealed an overall root-mean-square distance (RMSD) of 2.045 Å over 623 Cα atoms (Figure 7A). Although the UVR8^{W285A} from RUP2-UVR8^{W285A} and the UV-B-activated UVR8 from COP1^{WD40}-UVR8 show nearly identical conformations, with a RMSD of 0.381Å over 316 Cα atoms (Supplemental Figure 9A), RUP2 showed an overall shift of ∼5 Å in distance compared with COP1^{WD40} when the position of the bound UVR8 VP motif was used as a reference (Figure 7A). Notable differences can be observed in the two interaction interfaces. RUP2-UVR8^{W285A} exhibited a buried area of ∼1620 Å^2 with 31 pairs of residues forming hydrogen bond interactions (Figure 5A and Supplemental Figures 4A and 6A). By contrast, in the COP1^{WD40}-UVR8 complex, the observed counterpart area is ∼1399 Å^2 with 20 pairs of interacting residues (Wang et al., 2022).

Although differences exist in the RUP2-UVR8^{W285A} and COP1^{WD40}-UVR8 structures, the overall conformation of the C27 subregion-bound RUP2^{WD40} is almost identical to that of the VP motif-bound COP1^{WD40} (PDB: 7VGG and 6QTQ) (RMSD <0.7 Å over 215 Cα atoms) (Lau et al., 2019; Wang et al., 2022) (Supplemental Figure 8A and 8B). This suggests that these WD40 domains of RUP2 and COP1 share a common VP motif binding mode (Supplemental Figure 8C). In addition, four charged residues (R393, E442, E458, and E460) in COP1 are also conserved in RUP2 (R62, D122, E138, and D140) (Figure 7B) (Wang et al., 2022). RUP2 mutants with individual mutations in these four conserved residues can neither outcompete COP1 and separate it from UVR8 nor facilitate UVR8 redimerization (Wang et al., 2022).

Various UVR8 core domain structures have been reported previously, including ground state UVR8 (PDB: 4DNW), UVR8^{W285A} (PDB: 4DNU), and UV-B-activated UVR8 in COP1^{WD40}-UVR8 (PDB: 7VGG) (Wu et al., 2012; Wang et al., 2022). We further compared the UVR8^{W285A} structure from RUP2-UVR8^{W285A} with those reported UVR8 core domain structures. The overall structure of these core domains is nearly identical, and the most noticeable differences are observed in the side chain conformations of residues D129, W233, R234, and W337, which are involved in UV-B perception and electron-coupled proton transfer in wild-type UVR8 (Supplemental Figure 9). Compared with UVR8^{W285A} (PDB: 4DNU) and UV-B-activated UVR8 from COP1^{WD40}-UVR8 (PDB: 7VGG), the orientations of UVR8^{W285A}
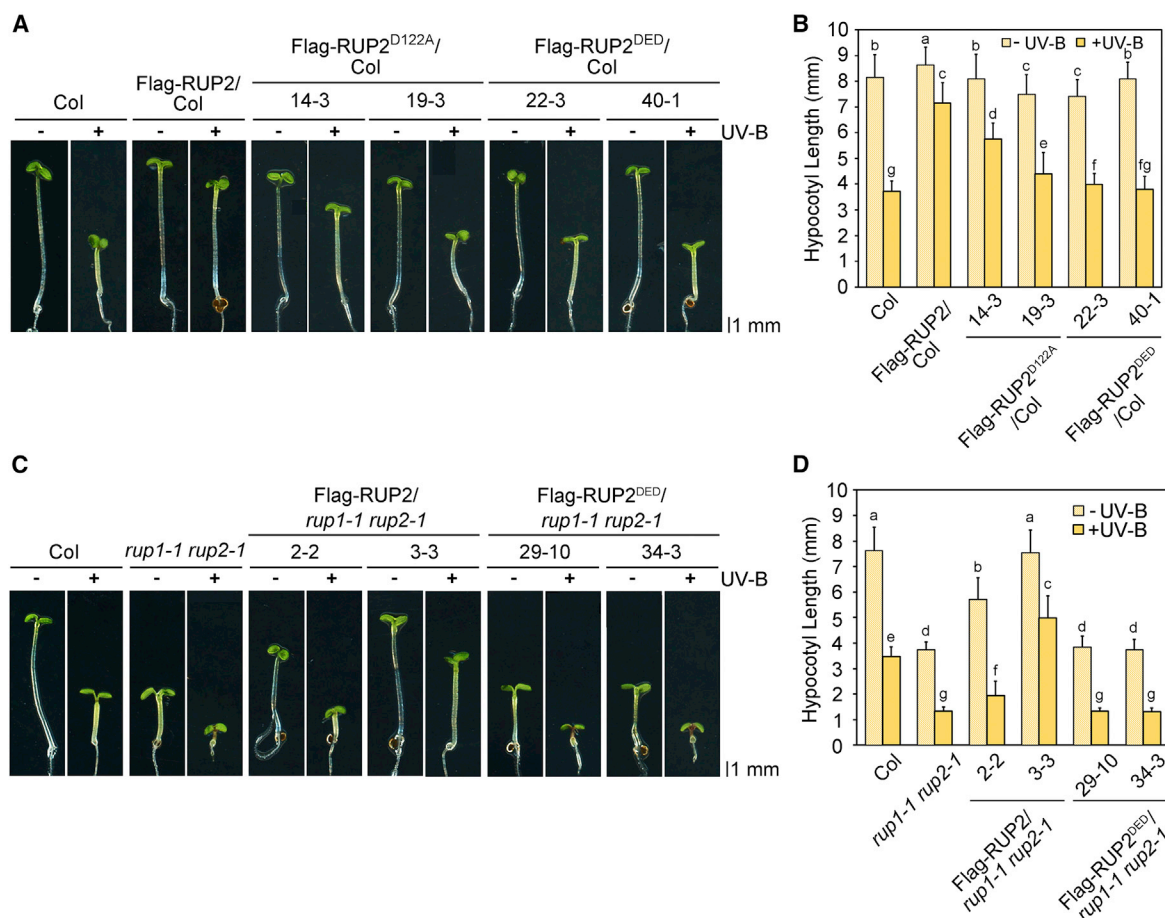
Figure 6. Mutations in RUP2 impair UVR8 redimerization *in planta*.

(A) Phenotypes of 4-day-old Col, Flag-RUP2/Col, Flag-RUP2^{D122A}/Col, and Flag-RUP2^{DED}/Col Arabidopsis seedlings grown with (+) or without (−) UV-B light exposure.

(B) Hypocotyl lengths of the seedlings shown in **(A)**. Mean ± SD, n ≥ 30. Different letters represent significant differences (p < 0.05, Student's t test) between samples.

(C) Phenotypes of 4-d-old Col, *rup1-1 rup2-1*, Flag-RUP2/*rup1-1 rup2-1*, and Flag-RUP2^{DED}/*rup1-1 rup2-1* Arabidopsis seedlings grown with (+) or without (−) UV-B light exposure.

(D) Hypocotyl lengths of the seedlings shown in **(C)**. Mean ± SD, n ≥ 30. Different letters represent significant differences (p < 0.05, Student's t test) between samples.

D129, W233, and W337 side chains in RUP2-UVR8^{W285A} are more similar to those of UVR8 in the ground state (PDB: 4DNW). Specifically, the hydrogen bond distance between UVR8^{W285A} D129 and W233 in RUP2-UVR8^{W285A} (2.9 Å) is comparable to that in dimeric UVR8 (2.8 Å), whereas those in UVR8^{W285A} (PDB: 4DNU) and COP1^{WD40}-UVR8 are 5.8 Å and 6.7 Å, respectively (Supplemental Figures 9 and 10A). As UVR8 D129 is involved in the COP1^{WD40}-UVR8 interaction and reported to function in electron-coupled proton-transfer-mediated UVR8 monomerization (Li et al., 2014, 2022; Wu et al., 2014; Wang et al., 2022), we wondered whether this residue is involved in UVR8 redimerization. In gel filtration chromatography, UVR8^{D129A} was characterized as a dimer in the absence of UV-B exposure, whereas UV-B activated UVR8^{D129A} appeared to be monomeric. However, UVR8^{D129A} was present as monomers on SDS-PAGE regardless of UV-B treatment, similar to UVR8^{W285A} (Supplemental Figure 10B). Thus, we used the gel filtration chromatography method to analyze the redimerization of UVR8^{D129A}. Most of the monomeric

wild-type UVR8 reverted to the dimeric state at 24 h post UV-B exposure. By contrast, only a small portion of the monomeric UVR8^{D129A} redimerized within the same time frame (Supplemental Figure 10C). These results suggest that D129 plays an important role in UVR8 redimerization.

DISCUSSION

UVR8-mediated UV-B signal transduction pathways play crucial roles in plant growth and development (Yin and Ulm, 2017; Liang et al., 2019; Podolec et al., 2021a). Multiple molecular players are involved in regulation of the UVR8-mediated UV-B response, and the RUP1/2-mediated facilitation of UVR8 ground state reversion is an integral part of the UVR8 photocycle (Yin and Ulm, 2017; Liang et al., 2019; Podolec et al., 2021a). Previous studies suggested that the UVR8 core domain and C-terminal tail are responsible for UV-B perception and signal transduction functions, respectively, and highlighted the importance of the C-terminal domain in RUP-UVR8 interaction (Christie et al., 2012; Wu
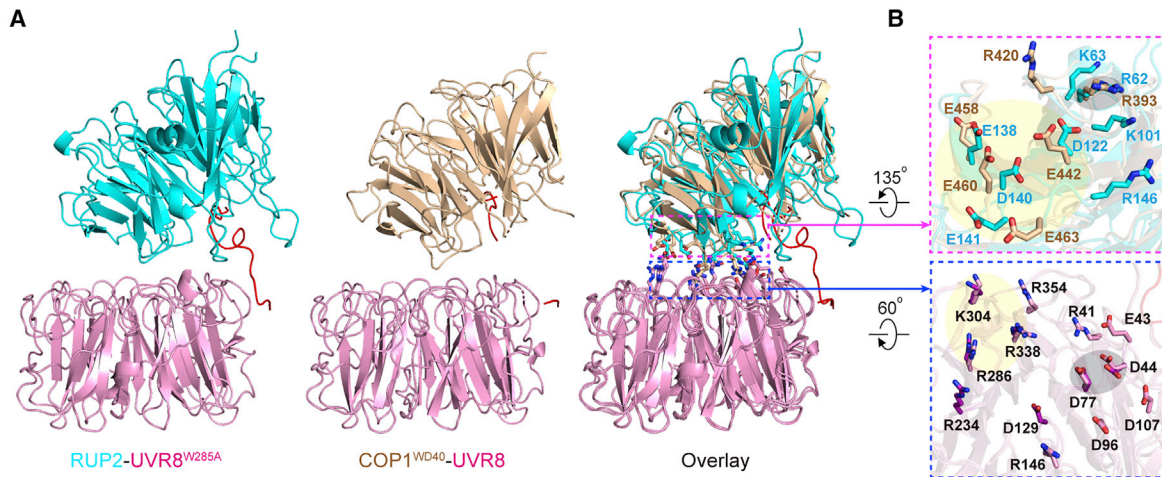
Figure 7. Structural comparison of the RUP2-UVR8^{W285A} complex and the COP1^{WD40}-UVR8 complex.
(A) Superposition of RUP2-UVR8^{W285A} and COP1^{WD40}-UVR8 (PDB: 7VGG). The core domain and C27 subregion of UVR8^{W285A} are indicated by pink and red, respectively. RUP2^{WD40} and COP1^{WD40} are colored in cyan and wheat, respectively.
(B) Close-up view of the charged residues in the two surface patches of RUP2 (in cyan, upper panel) and COP1^{WD40} (in wheat, upper panel), or UVR8^{W285A} (in pink, lower panel) and UV-B activated UVR8 (in purple, lower panel), respectively. The conserved residues illustrated with a yellow undertone are the negatively charged RUP2 residues D122, E138, D140, and E141 and the corresponding COP1^{WD40} E442, E458, E460, and E463. The conserved residues illustrated with a gray undertone are the positively charged RUP2 R62 and the corresponding COP1^{WD40} R393. The charged residues R286, K304, R338, D44, and D77 of UVR8 are involved in the interactions with both RUP2 and COP1^{WD40}.

et al., 2012; Yin et al., 2015; Lau et al., 2019; Podolec et al., 2021a; Wang et al., 2022). Here, through structural determination of the RUP2-UVR8^{W285A} complex and biochemical analysis, we found that in addition to the C-terminal domain, the UVR8 core domain is also involved in the RUP2-UVR8 interaction. The importance of both interaction interfaces for RUP2-mediated facilitation of UVR8 redimerization was also verified.

Notably, RUP2 facilitates the reversion of active state UVR8 to the ground state (monomer to dimer), yet RUP2 occupies the UVR8 dimer surface in the RUP2-UVR8^{W285A} complex. Our findings suggest that the UVR8 core domain should dissociate from RUPs prior to homodimer formation. The RUP2-mediated facilitation of UVR8 redimerization is a highly dynamic process (Figure 1B and 1C). We speculate that different intermediate states in which RUP2 interacts with monomeric/homodimeric UVR8 are likely to exist. The mode of action underlying RUP-UVR8 dissociation and UVR8 dimer formation remains to be further investigated.

In UVR8-mediated UV-B signaling pathways, active state UVR8 forms the UVR8-COP1/SPA complex, eventually leading to positive regulation of UV-B responses (Oravecz et al., 2006; Favory et al., 2009; Rizzini et al., 2011; Cloix et al., 2012; Heijde et al., 2013; Huang et al., 2014; Yin et al., 2015; Wang et al., 2022). As negative feedback regulators, RUPs disrupt the UVR8-COP1/SPA complex and facilitate UVR8 ground state reversion to repress UV-B signal transduction (Gruber et al., 2010; Heijde and Ulm, 2013; Podolec et al., 2021a; Wang et al., 2022). Interestingly, RUP2-UVR8^{W285A} and the recently reported COP1^{WD40}-UVR8 adopt a similar overall architecture, and the COP1^{WD40} domain also interacts with both the UVR8 core and C-terminal domains (Wang et al., 2022) (Figure 7). These findings suggest that a common interaction mode (with a similar molecular basis) might be shared by molecular

regulators of UVR8 involved in the UVR8 photocycle. In addition, compared with the COP1^{WD40}-UVR8 complex, the RUP2-UVR8^{W285A} complex has larger buried surface areas harboring more interacting residues, suggesting that RUP2 might have stronger binding affinity than COP1 to UVR8. This could explain why RUP2 can dissociate UVR8 from the COP1-UVR8 complex (Wang et al., 2022).

In summary, we report the two-interface interaction of RUP2 and UVR8, an interaction mode also adopted by COP1 and UVR8, and verified the functional importance of both RUP2-UVR8 interaction interfaces. Although how RUPs facilitate the redimerization of UVR8 remains to be further elucidated, our findings mark a step forward in understanding the molecular basis that underpins the interactions between UVR8 and its photocycle regulators.

MATERIALS AND METHODS

Molecular cloning and protein expression

Full-length *RUP1*, *RUP2*, and *UVR8* genes were amplified from the *A. thaliana* cDNA library using standard PCR-based cloning strategies. *RUP2* and *UVR8* mutants were amplified by Fusion PCR. Full-length *RUP1*, *RUP2*, and *RUP2* mutants were subcloned into a modified pMlink vector (Lu et al., 2014) containing a C-terminal 3×Flag tandem affinity tag. Full-length *UVR8^{W285A}* and mutants based on *UVR8^{W285A}* were subcloned into the pMlink vector with a C-terminal Twin-Strep-tag. All clones were verified by sequencing. Proteins were expressed in Expi293F mammalian cells (Invitrogen) (a new, suspension-adapted [human embryonic kidney 293] HEK293 cell line), as previously described (Wang et al., 2022). Plasmids encoding RUP2 (residues 21–366) and UVR8^{W285A} (residues 12–421) were co-transfected into cells with polyethylenimines (PEIs) (Polysciences). Transfected cells were cultured for 60 h before harvesting. The cells were collected by centrifugation at 1500 × *g* for 15 min. The cell pellet was subsequently washed with PBS and resuspended in lysis buffer A containing 50 mM Tris-HCl (pH 8.0) and 150 mM NaCl. The cell suspensions were flash-frozen in liquid nitrogen and stored at −80°C.

Protein purification

The stored cell suspension was thawed at room temperature and lysed using a JN-02 homogenizer (JNBIO, China). The lysed cells were ultracentrifuged at 20 000 × g at 4°C for 1 h to remove the cell pellets. The supernatant was incubated with anti-Flag G1 affinity resin (GenScript) at 4°C for 2 h. The bound proteins were washed with 5 column volumes (CVs) of buffer A and then eluted with buffer A containing 300 μg ml^{-1} Flag peptide (Genscript). The eluted protein was further purified by anion-exchange chromatography (Source 15Q 10/100, GE Healthcare). The protein was concentrated with a 10-kDa cutoff Centricon (Millipore) and then subjected to size-exclusion chromatography (Superdex-200 Increase 10/300, GE Healthcare) in buffer containing 25 mM Tris-HCl (pH 8.0), 150 mM NaCl, and 5 mM dithiothreitol (DTT). The homogeneous peak fractions of RUP2-UVR8^{W285A} were pooled and immediately used for crystallization.

For *in vitro* biochemical assays, the wild-type and mutant *UVR8* genes were subcloned into a modified pET15 vector with an N-terminal 6×His tag followed by a drICE protease cleavage site. The fusion proteins were expressed in *Escherichia coli* cell strain BL21 (DE3) and purified as described previously (Ma et al., 2020b). The proteins were digested by drICE protease before size-exclusion chromatography.

Crystallization

The sitting drop or hanging drop vapor diffusion method (18°C) was used for crystallization. Crystals of the RUP2-UVR8^{W285A} complex were obtained from drops containing a mixture of 1 μL protein (6.7 mg mL^{-1} in storage buffer) and 1 μL of crystallization buffer containing 14.8% (w/v) PEG 6000, 100 mM MES (pH 5.5), 62.5 mM NH$_4$Cl, 10 mM hexamminecobalt (III) chloride, and 2% sucrose. High-quality crystals were flash-frozen in liquid nitrogen and cryoprotected by adding 25% (v/v) ethylene glycol.

Data collection and structure determination

All diffraction data for the RUP2-UVR8^{W285A} complex were collected at the Shanghai Synchrotron Radiation Facility on beamline BL17U or BL19U using a CCD detector cooled to 100K. The diffraction data were processed using the HKL2000 program suite and XDS packages (Otwinowski and Minor, 1997). Further data processing was carried out using the CCP4 suite (Winn et al., 2011). The structure was iteratively built using COOT (Emsley and Cowtan, 2004) and refined with the PHENIX program (Adams et al., 2010). Data collection and structure refinement statistics are summarized in Supplemental Table 1. All figures representing structures were generated using PyMOL (http://www.pymol.org/).

Redimerization of wild-type UVR8 or UVR8 variants mediated by RUP2

UV-B treatment and redimerization of UV-B-activated wild-type UVR8 or UVR8 variants (UVR8^{N396} and UVR8^{D44A}) were performed as described previously (Wang et al., 2022). Equal volumes of the reaction products were sampled at different time points and subjected to SDS-PAGE (i.e., the total amount of UVR8 [monomeric and homodimeric UVR8] loaded in each lane was the same). To quantify the kinetics of dimer regeneration of wild-type UVR8 or UVR8 variants, the band intensity of redimerized UVR8/variants was measured on Coomassie-stained gels with ImageJ software. The percentage of redimerized UVR8 relative to the dimer without UV-B illumination at a given time point was plotted and fitted using Nonlinear Curve Fitting in OriginPro 2021.

Pull-down assays

Expi293F cells expressing RUP1/2-Flag or UVR8/UVR8^{W285A}-Strep II were harvested and washed with PBS buffer. The cells expressing RUP1/2-Flag were then lysed in buffer A by repeated freezing-thawing three times and centrifuged at 4°C and 18 000 × g for 1 h. The supernatant was incubated with anti-Flag G1 affinity resin (GenScript) at 4°C for 2 h. The bound proteins were washed with 5 CVs of buffer A and eluted with

buffer A containing 300 μg mL^{-1} Flag peptide (Genscript). The cells expressing UVR8/UVR8^{W285A}-Strep II were lysed in buffer B containing 100 mM Tris-HCl (pH 8.0), 150 mM NaCl, and 1 mM EDTA and purified with Strep-Tactin (IBA) affinity resin as for Flag affinity purification. The bound proteins were washed with 5 CVs of buffer B and eluted with buffer B containing 2.5 mM D-desthiobiotin (IBA).

For Flag pull-down assays, a mixture of 100 μg UVR8/UVR8^{W285A}-Strep II and 250 μg RUP1/RUP2-Flag was incubated with 150 μL anti-Flag G1 affinity resin (GenScript) under UV-B irradiation (for UVR8-Strep II) or in the dark (for UVR8^{W285A}-Strep II) in buffer A at room temperature for 30 min. The bound protein was washed with 5 CVs of buffer A and then eluted using buffer B containing 300 μg mL^{-1} Flag peptide (Genscript). These input samples were analyzed by SDS-PAGE. Proteins from elution fractions were detected by immunoblotting with antibodies against Strep II or Flag (all antibodies were used at a 1:3000 dilution).

Immunoblot assays

Expi293F cells co-expressing UVR8^{W285A}-Strep II and RUP2 mutants-Flag were lysed in lysis buffer B by repeated freezing-thawing three times. The proteins were purified using the Strep II-tag protein purification method mentioned above. Cells co-expressing UVR8^{W285A} mutants-Strep II and wild-type RUP2-Flag were lysed in buffer A. The proteins were purified using the Flag-tag protein purification method mentioned above. Cell lysis supernatants were detected by immunoblotting with antibodies against Strep II and Flag (all antibodies were used at a 1:3000 dilution). Proteins from elution fractions were analyzed by SDS-PAGE.

Gel filtration chromatography analysis

The dimer or monomer state of UVR8 and UVR8^{D129A} was determined by gel filtration chromatography analysis. Samples were then injected into a Superdex 200 Increase 10/30 GL column (GE Healthcare) equilibrated with buffer containing 25 mM Tris-HCl (pH 8.0), 150 mM NaCl, and 5 mM DTT. Data analysis was performed using GraphPad Prism8.

Plant materials and growth conditions

The wild-type *A. thaliana* lines used in this study were in the Columbia (Col) background. Flag-RUP2/Col and *rup1-1 rup2-1* were described previously (Ren et al., 2019). Transgenic Flag-RUP2/*rup1-1 rup2-1*, Flag-RUP2^{DED}/*rup1-1 rup2-1*, Flag-RUP2^{D122A}/Col, and Flag-RUP2^{DED}/Col plants were generated by the floral dip method using *Agrobacterium* strain GV3101.

The seeds were surface-sterilized and sown on solid 1% Murashige and Skoog medium supplemented with 1% sucrose for molecular and biochemical assays or with 0.3% sucrose for phenotypic analysis, followed by cold treatment at 4°C for 4 days before light treatment. For UV-B-induced photomorphogenesis, seedlings were grown at 22°C under continuous low white light (3 μmol·m^{-2}·s^{-1}, measured by an HR-350 Light Meter, Hipoint) supplemented with UV-B light from Philips TL20W/01RS narrowband UV-B tubes (1.5 μmol·m^{-2}·s^{-1}, measured by a UV-297 UV-B Light Meter, HANDY) under a 350-nm cutoff (half-maximal transmission at 350 nm) ZUL0350 filter (−UV-B; Asahi spectra) or a 300-nm cutoff (half-maximal transmission at 300 nm) ZUL0300 filter (+UV-B; Asahi spectra).

Hypocotyl measurement

Hypocotyl length was measured as described previously (Ren et al., 2019). For each line grown under −UV-B or +UV-B for 4 days, hypocotyl length was analyzed for three biological replicates, each consisting of at least 30 *Arabidopsis* seedlings. Hypocotyl length was quantified using ImageJ (http://rsb.info.nih.gov/ij/).

AUTHOR CONTRIBUTIONS

P.Y. conceived the project. L.W., Y.W., and P.Y. designed all experiments. Y.W. and H.C. performed protein purification and crystallization. Z.G. determined the structure. L.W., Y.W., H.C., L.M., and D.Z. performed the biochemical assays. X.H., H.R., X.W. and J.W. designed and performed the in planta assays. All authors analyzed the data and contributed to manuscript preparation. L.W., Y.W., and P.Y. wrote the manuscript.

REFERENCES

Adams, P.D., Afonine, P.V., Bunkóczi, G., Chen, V.B., Davis, I.W., Echols, N., Headd, J.J., Hung, L.W., Kapral, G.J., Grosse-Kunstleve, R.W., et al. (2010). PHENIX: a comprehensive Python-based system for macromolecular structure solution. Acta Crystallogr. D Biol. Crystallogr. **66**:213–221. https://doi.org/10.1107/S0907444909052925.

Binkert, M., Kozma-Bognár, L., Terecskei, K., De Veylder, L., Nagy, F., and Ulm, R. (2014). UV-B-responsive association of the Arabidopsis bZIP transcription factor ELONGATED HYPOCOTYL5 with target genes, including its own promoter. Plant Cell **26**:4200–4213. https://doi.org/10.1105/tpc.114.130716.

Christie, J.M., Arvai, A.S., Baxter, K.J., Heilmann, M., Pratt, A.J., O'Hara, A., Kelly, S.M., Hothorn, M., Smith, B.O., Hitomi, K., et al. (2012). Plant UVR8 photoreceptor senses UV-B by tryptophan-mediated disruption of cross-dimer salt bridges. Science **335**:1492–1496. https://doi.org/10.1126/science.1218091.

Cloix, C., Kaiserli, E., Heilmann, M., Baxter, K.J., Brown, B.A., O'Hara, A., Smith, B.O., Christie, J.M., and Jenkins, G.I. (2012). C-terminal region of the UV-B photoreceptor UVR8 initiates signaling through interaction with the COP1 protein. Proc. Natl. Acad. Sci. USA. **109**:16366–16370. https://doi.org/10.1073/pnas.1210898109.

Emsley, P., and Cowtan, K. (2004). Coot: model-building tools for molecular graphics. Acta Crystallogr. D Biol. Crystallogr. **60**:2126–2132. https://doi.org/10.1107/S0907444904019158.

Favory, J.J., Stec, A., Gruber, H., Rizzini, L., Oravecz, A., Funk, M., Albert, A., Cloix, C., Jenkins, G.I., Oakeley, E.J., et al. (2009). Interaction of COP1 and UVR8 regulates UV-B-induced photomorphogenesis and stress acclimation in Arabidopsis. EMBO J. **28**:591–601. https://doi.org/10.1038/emboj.2009.4.

Gruber, H., Heijde, M., Heller, W., Albert, A., Seidlitz, H.K., and Ulm, R. (2010). Negative feedback regulation of UV-B-induced photomorphogenesis and stress acclimation in Arabidopsis. Proc. Natl. Acad. Sci. USA. **107**:20132–20137. https://doi.org/10.1073/pnas.0914532107.

Han, X., Huang, X., and Deng, X.W. (2020). The photomorphogenic central repressor COP1: conservation and functional diversification during evolution. Plant Commun. **1**:100044. https://doi.org/10.1016/j.xplc.2020.100044.

Heijde, M., and Ulm, R. (2012). UV-B photoreceptor-mediated signalling in plants. Trends Plant Sci. **17**:230–237. https://doi.org/10.1016/j.tplants.2012.01.007.

Heijde, M., and Ulm, R. (2013). Reversion of the Arabidopsis UV-B photoreceptor UVR8 to the homodimeric ground state. Proc. Natl. Acad. Sci. USA. **110**:1113–1118. https://doi.org/10.1073/pnas.1214237110.

Heijde, M., Binkert, M., Yin, R., Ares-Orpel, F., Rizzini, L., Van De Slijke, E., Persiau, G., Nolf, J., Gevaert, K., De Jaeger, G., et al. (2013). Constitutively active UVR8 photoreceptor variant in Arabidopsis. Proc. Natl. Acad. Sci. USA. **110**:20326–20331. https://doi.org/10.1073/pnas.1314336110.

Heilmann, M., and Jenkins, G.I. (2013). Rapid reversion from monomer to dimer regenerates the ultraviolet-B photoreceptor UV RESISTANCE LOCUS8 in intact Arabidopsis plants. Plant Physiol. **161**:547–555. https://doi.org/10.1104/pp.112.206805.

Holm, M., Hardtke, C.S., Gaudet, R., and Deng, X.W. (2001). Identification of a structural motif that confers specific interaction with the WD40 repeat domain of Arabidopsis COP1. EMBO J. **20**:118–127. https://doi.org/10.1093/emboj/20.1.118.

Huang, X., Ouyang, X., Yang, P., Lau, O.S., Chen, L., Wei, N., and Deng, X.W. (2013). Conversion from CUL4-based COP1-SPA E3 apparatus to UVR8-COP1-SPA complexes underlies a distinct biochemical function of COP1 under UV-B. Proc. Natl. Acad. Sci. USA. **110**:16669–16674. https://doi.org/10.1073/pnas.1316622110.

Huang, X., Yang, P., Ouyang, X., Chen, L., and Deng, X.W. (2014). Photoactivated UVR8-COP1 module determines photomorphogenic UV-B signaling output in Arabidopsis. PLoS Genet. **10**:e1004218. https://doi.org/10.1371/journal.pgen.1004218.

Jenkins, G.I. (2009). Signal transduction in responses to UV-B radiation. Annu. Rev. Plant Biol. **60**:407–431. https://doi.org/10.1146/annurev.arplant.59.032607.092953.

Jiang, J., Liu, J., Sanders, D., Qian, S., Ren, W., Song, J., Liu, F., and Zhong, X. (2021). UVR8 interacts with de novo DNA methyltransferase and suppresses DNA methylation in Arabidopsis. Nat. Plants **7**:184–197. https://doi.org/10.1038/s41477-020-00843-4.

Kliebenstein, D.J., Lim, J.E., Landry, L.G., and Last, R.L. (2002). Arabidopsis UVR8 regulates ultraviolet-B signal transduction and tolerance and contains sequence similarity to human regulator of chromatin condensation 1. Plant Physiol. **130**:234–243. https://doi.org/10.1104/pp.234.

Lau, K., Podolec, R., Chappuis, R., Ulm, R., and Hothorn, M. (2019). Plant photoreceptors and their signaling components compete for COP1 binding via VP peptide motifs. EMBO J. **38**:e102140. https://doi.org/10.15252/embj.2019102140.

Li, X., Chung, L.W., Morokuma, K., and Li, G. (2014). Theoretical study on the UVR8 photoreceptor: sensing ultraviolet-B by tryptophan and dissociation of homodimer. J. Chem. Theory Comput. **10**:3319–3330. https://doi.org/10.1021/ct5003362.

Li, X., Liu, Z., Ren, H., Kundu, M., Zhong, F.W., Wang, L., Gao, J., and Zhong, D. (2022). Dynamics and mechanism of dimer dissociation of photoreceptor UVR8. Nat. Commun. **13**:93. https://doi.org/10.1038/s41467-021-27756-w.

Li, X., Ren, H., Kundu, M., Liu, Z., Zhong, F.W., Wang, L., Gao, J., and Zhong, D. (2020). A leap in quantum efficiency through light harvesting in photoreceptor UVR8. Nat. Commun. **11**:4316. https://doi.org/10.1038/s41467-020-17838-6.

Liang, T., Mei, S., Shi, C., Yang, Y., Peng, Y., Ma, L., Wang, F., Li, X., Huang, X., Yin, Y., et al. (2018). UVR8 interacts with BES1 and BIM1 to regulate transcription and photomorphogenesis in Arabidopsis. Dev. Cell **44**:512–523.e5. https://doi.org/10.1016/j.devcel.2017.12.028.

Liang, T., Yang, Y., and Liu, H. (2019). Signal transduction mediated by the plant UV-B photoreceptor UVR8. New Phytol. **221**:1247–1252. https://doi.org/10.1111/nph.15469.

Lin, L., Dong, H., Yang, G., and Yin, R. (2020). The C-terminal 17 amino acids of the photoreceptor UVR8 is involved in the fine-tuning of UV-B signaling. J. Integr. Plant Biol. **62**:1327–1340. https://doi.org/10.1111/jipb.12977.

Lu, P., Bai, X.C., Ma, D., Xie, T., Yan, C., Sun, L., Yang, G., Zhao, Y., Zhou, R., Scheres, S.H.W., et al. (2014). Three-dimensional structure of human gamma-secretase. Nature **512**:166–170. https://doi.org/10.1038/nature13567.

Ma, L., Guan, Z., Wang, Q., Yan, X., Wang, J., Wang, Z., Cao, J., Zhang, D., Gong, X., and Yin, P. (2020a). Structural insights into the photoactivation of Arabidopsis CRY2. Nat. Plants **6**:1432–1438. https://doi.org/10.1038/s41477-020-00800-1.

Ma, L., Wang, X., Guan, Z., Wang, L., Wang, Y., Zheng, L., Gong, Z., Shen, C., Wang, J., Zhang, D., et al. (2020b). Structural insights into BIC-mediated inactivation of Arabidopsis cryptochrome 2. Nat. Struct. Mol. Biol. **27**:472–479. https://doi.org/10.1038/s41594-020-0410-z.

Mathes, T., Heilmann, M., Pandit, A., Zhu, J., Ravensbergen, J., Kloz, M., Fu, Y., Smith, B.O., Christie, J.M., Jenkins, G.I., et al. (2015). Proton-coupled electron transfer constitutes the photoactivation mechanism of the plant photoreceptor UVR8. J. Am. Chem. Soc. **137**:8113–8120. https://doi.org/10.1021/jacs.5b01177.

Oravecz, A., Baumann, A., Máté, Z., Brzezinska, A., Molinier, J., Oakeley, E.J., Ádám, E., Schäfer, E., Nagy, F., and Ulm, R. (2006). CONSTITUTIVELY PHOTOMORPHOGENIC1 is required for the UV-B response in Arabidopsis. Plant Cell **18**:1975–1990. https://doi.org/10.1105/tpc.105.040097.

Otwinowski, Z., and Minor, W. (1997). Processing of X-ray diffraction data collected in oscillation mode. Methods Enzymol. **276**:307–326.

Podolec, R., Demarsy, E., and Ulm, R. (2021a). Perception and signaling of ultraviolet-B radiation in plants. Annu. Rev. Plant Biol. **72**:793–822. https://doi.org/10.1146/annurev-arplant-050718-095946.

Podolec, R., Lau, K., Wagnon, T.B., Hothorn, M., and Ulm, R. (2021b). A constitutively monomeric UVR8 photoreceptor confers enhanced UV-B photomorphogenesis. Proc. Natl. Acad. Sci. USA. **118**. https://doi.org/10.1073/pnas.2017284118.

Qian, C., Chen, Z., Liu, Q., Mao, W., Chen, Y., Tian, W., Liu, Y., Han, J., Ouyang, X., and Huang, X. (2020). Coordinated transcriptional regulation by the UV-B photoreceptor and multiple transcription factors for plant UV-B responses. Mol. Plant **13**:777–792. https://doi.org/10.1016/j.molp.2020.02.015.

Ren, H., Han, J., Yang, P., Mao, W., Liu, X., Qiu, L., Qian, C., Liu, Y., Chen, Z., Ouyang, X., et al. (2019). Two E3 ligases antagonistically regulate the UV-B response in Arabidopsis. Proc. Natl. Acad. Sci. USA. **116**:4722–4731. https://doi.org/10.1073/pnas.1816268116.

Rizzini, L., Favory, J.J., Cloix, C., Faggionato, D., O'Hara, A., Kaiserli, E., Baumeister, R., Schäfer, E., Nagy, F., Jenkins, G.I., et al. (2011).

Perception of UV-B by the Arabidopsis UVR8 protein. Science **332**:103–106. https://doi.org/10.1126/science.1200660.

Rozema, J., van de Staaij, J., Björn, L.O., and Caldwell, M. (1997). UV-B as an environmental factor in plant life: stress and regulation. Trends Ecol. Evol. **12**:22–28. https://doi.org/10.1016/s0169-5347(96)10062-8.

Shao, K., Zhang, X., Li, X., Hao, Y., Huang, X., Ma, M., Zhang, M., Yu, F., Liu, H., and Zhang, P. (2020). The oligomeric structures of plant cryptochromes. Nat. Struct. Mol. Biol. **27**:480–488. https://doi.org/10.1038/s41594-020-0420-x.

Ulm, R., Baumann, A., Oravecz, A., Máté, Z., Ádám, E., Oakeley, E.J., Schäfer, E., and Nagy, F. (2004). Genome-wide analysis of gene expression reveals function of the bZIP transcription factor HY5 in the UV-B response of Arabidopsis. Proc. Natl. Acad. Sci. USA. **101**:1397–1402. https://doi.org/10.1073/pnas.0308044100.

Voityuk, A.A., Marcus, R.A., and Michel-Beyerle, M.E. (2014). On the mechanism of photoinduced dimer dissociation in the plant UVR8 photoreceptor. Proc. Natl. Acad. Sci. USA. **111**:5219–5224. https://doi.org/10.1073/pnas.1402025111.

Wang, Y., Wang, L., Guan, Z., Chang, H., Ma, L., Shen, C., Qiu, L., Yan, J., Zhang, D., Li, J., et al. (2022). Structural insight into UV-B-activated UVR8 bound to COP1. Sci. Adv. **8**:eabn3337. https://doi.org/10.1126/sciadv.abn3337.

Winn, M.D., Ballard, C.C., Cowtan, K.D., Dodson, E.J., Emsley, P., Evans, P.R., Keegan, R.M., Krissinel, E.B., Leslie, A.G.W., McCoy, A., et al. (2011). Overview of the CCP4 suite and current developments. Acta Crystallogr. D Biol. Crystallogr. **67**:235–242. https://doi.org/10.1107/S0907444910045749.

Wu, D., Hu, Q., Yan, Z., Chen, W., Yan, C., Huang, X., Zhang, J., Yang, P., Deng, H., Wang, J., et al. (2012). Structural basis of ultraviolet-B perception by UVR8. Nature **484**:214–219. https://doi.org/10.1038/nature10931.

Wu, M., Farkas, D., Eriksson, L.A., and Strid, Å. (2019). Proline 411 biases the conformation of the intrinsically disordered plant UVR8 photoreceptor C27 domain altering the functional properties of the peptide. Sci. Rep. **9**:818. https://doi.org/10.1038/s41598-018-37005-8.

Wu, M., Strid, Å., and Eriksson, L.A. (2014). Photochemical reaction mechanism of UV-B-induced monomerization of UVR8 dimers as the first signaling event in UV-B-regulated gene expression in plants. J. Phys. Chem. B **118**:951–965. https://doi.org/10.1021/jp4104118.

Yang, X., Montano, S., and Ren, Z. (2015). How does photoreceptor UVR8 perceive a UV-B signal? Photochem. Photobiol. **91**:993–1003. https://doi.org/10.1111/php.12470.

Yang, Y., Liang, T., Zhang, L., Shao, K., Gu, X., Shang, R., Shi, N., Li, X., Zhang, P., and Liu, H. (2018). UVR8 interacts with WRKY36 to regulate HY5 transcription and hypocotyl elongation in Arabidopsis. Nat. Plants **4**:98–107. https://doi.org/10.1038/s41477-017-0099-0.

Yang, Y., Zhang, L., Chen, P., Liang, T., Li, X., and Liu, H. (2020). UV-B photoreceptor UVR8 interacts with MYB73/MYB77 to regulate auxin responses and lateral root development. EMBO J. **39**:e101928. https://doi.org/10.15252/embj.2019101928.

Yin, R., and Ulm, R. (2017). How plants cope with UV-B: from perception to response. Curr. Opin. Plant Biol. **37**:42–48. https://doi.org/10.1016/j.pbi.2017.03.013.

Yin, R., Arongaus, A.B., Binkert, M., and Ulm, R. (2015). Two distinct domains of the UVR8 photoreceptor interact with COP1 to initiate UV-B signaling in Arabidopsis. Plant Cell **27**:202–213. https://doi.org/10.1105/tpc.114.133868.